J. Fluid Mech. (1977), *vol.* 82, *part* 2, *pp.* 209–222
Printed in Great Britain

Numerical analysis of turbulent end-wall boundary layers of intense vortices

By JOSEPH CHI†
National Bureau of Standards, Washington, D.C. 20234

(Received 6 July 1976 and in revised form 22 March 1977)

After a careful consideration of the laws of generation, advection, diffusion and dissipation of turbulent kinetic energy proposed by Prandtl (1945) and Emmons (1954), equations of motion and turbulent kinetic energy for the vortex flow near a solid end wall are established. These equations are then evaluated by a numerical procedure. Care is taken to specify boundary conditions such that satisfactory matching of the solution with the main vortex is assured. The agreement between the predicted mean velocity distribution and the experimental data is remarkably good. In addition, several interesting characteristics are predicted by the theory: (i) the vertical distribution of horizontal velocity is oscillatory in the inner region, whilst it is of the ordinary boundary-layer type in the outer region; (ii) the maximum velocity in the boundary layer can exceed that in the main vortex by a considerable amount and (iii) the minimum pressure of the vortex does not occur in the vortex-core root as has been generally believed.

1. Introduction

Vortex boundary-layer flow on a solid wall like that shown in figure 1 occurs in many engineering situations such as the flows in the vicinity of the end walls of cyclones, Hilsch tubes and vaneless diffusers. In addition, a theory of the end-wall boundary-layer flow can assist an understanding of the flow near the ground in natural tornadoes and dust devils. Difficulties of the problem due to the nonlinearity of the governing equations and the rapid variation of the velocity of the main vortex were encountered by the early investigators. Because of these difficulties previous theoretical treatments of the vertical distribution of the velocity components in the vortex boundary layer have been limited to similar solutions, in which the tangential velocity of the main flow is given by the power law $v^+ \propto (r^+)^n$ and its radial velocity is assumed to be zero, e.g. see Bödewadt (1940), Stewartson (1957), Mack (1964) and Kuo (1971). These solutions are difficult if not impossible to match with the main vortex. An additional difficulty with vortex boundary-layer flow is that such flows are often turbulent and few attempts have been made to establish turbulent models.

An objective of this research is to bring the understanding of the turbulent vortex boundary layer up to the modern level of satisfaction. To achieve this, a numerical

† This work was carried out under NSF Grant GK41469 while the author was associated with the George Washington University so it does not represent an NBS publication; it is also noted that the author's name has been changed from S.W. Chi.

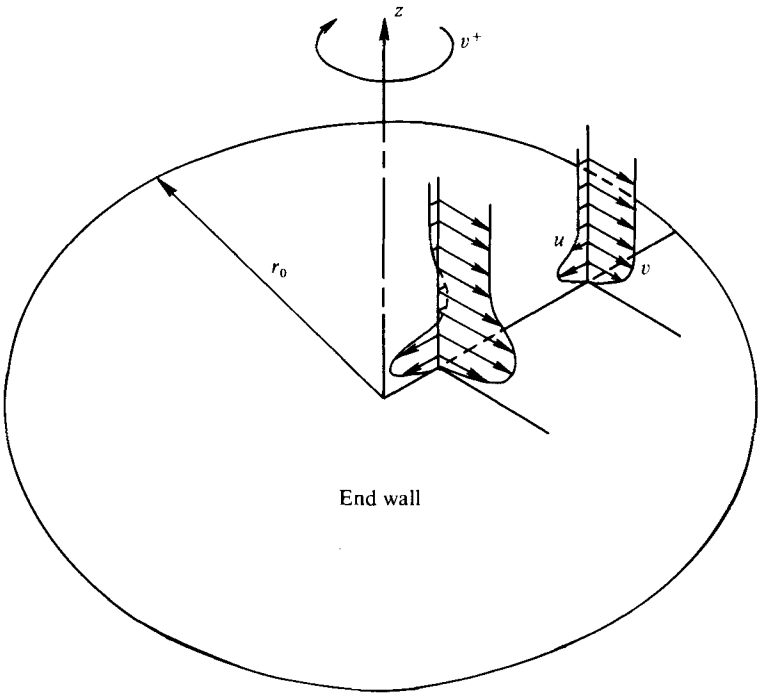

FIGURE 1. Sketch of turbulent end-wall boundary layer under investigation.

procedure for solving the full equations governing laminar vortex flow without simplifying assumptions was developed by Chi & Jih (1974), the requirements on the upper boundary conditions for satisfactory matching of the boundary-layer solution with the main vortex were established by Chi (1974), and measurements of the mean velocity distribution in a turbulent vortex boundary layer were made by Chi & Costopoulos (1974). Also, a preliminary examination of the turbulence theory was made by Chi & Glowacki (1974), but was limited to the region at large radius, far away from the vortex-core root.

This paper represents an attempt to extend the treatment of turbulent vortex boundary-layer flow to cover not only the region at large radius but also the vortex-core root. An important feature of the flow in a vortex boundary layer is that the turbulence which is generated in the remote high shear region of the boundary layer at large radius must be conveyed to the vortex-core root by the action of advection and diffusion. For quantitative evaluation of this feature, it is necessary to postulate mathematical relationships describing the processes of generation, advection, diffusion and dissipation of turbulent energy. Fortunately, there are several proposals which may be used, including those of Prandtl (1945), Emmons (1954), Glushko (1965) and Spalding (1967), although none of these authors has applied the equation to vortex flow.

In order to determine the length scales and the diffusion constant which appear in the postulated relationships for the generation, dissipation and diffusion of turbulent energy, it would be necessary to appeal to experimental data for the vortex boundary layer which are not available. However, as the present formulation is reducible to two-

dimensional flow, it is convenient to re-examine the data for zero-pressure and linear-shear layers, which have already been treated by Townsend (1961) and Spalding (1967) from a point of view which exhibits both similarity to and differences from that of the present paper.

With the length scales and the diffusion constant so determined, the full equations of motion and turbulent energy are solved by a numerical procedure without simplifying assumptions. Although the lack of turbulence measurements prevents a complete comparison of the present theory with experiments, the agreement of the present theory with the measured mean velocity has been found wholly satisfactory.

2. Vortex boundary-layer turbulence model

From the turbulence model proposed by Prandtl (1945), Emmons (1954), Glushko (1965) and Spalding (1967) for two dimensions, the equation describing the balance of advection, generation, diffusion and dissipation of turbulent kinetic energy for axisymmetric flow of an incompressible fluid (e.g. see Hinze 1959) can be written as

$$\underset{\text{Advection}}{[\rho(u\,\partial k/\partial r + w\,\partial k/\partial z)]} - \underset{\text{Generation}}{\mu_t\{2[(\partial u/\partial r)^2 + (\partial w/\partial z)^2] + (\partial u/\partial z + \partial w/\partial r)^2} + (\partial v/\partial z)^2 + r^2[\partial(u/r)/\partial r]^2\} - \{\underset{\text{Diffusion}}{\partial[(\mu+\gamma_t)\,\partial k/\partial z]/\partial z} + \partial[(\mu+\gamma_t)\,\partial k/\partial r]/\partial r\} + \underset{\text{Dissipation}}{\epsilon} = 0. \tag{1}$$

Also, the following laws can be used to describe the turbulent eddy viscosity μ_t, the diffusion coefficient γ_t and the dissipation ϵ respectively:

$$\mu_t = \rho l_\mu k^{\frac{1}{2}}, \quad \gamma_t = \mu_t/\sigma, \quad \epsilon = \rho k^{\frac{3}{2}}/l_D. \tag{2)–(4}$$

In the above equations, (u, v, w) and (u', v', w) are the components of the mean and fluctuating velocities, respectively, in the cylindrical co-ordinate system (r, θ, z) while k is the turbulent energy, defined as $\frac{1}{2}(\overline{u'^2}+\overline{v'^2}+\overline{w'^2})$, ρ the density, μ the laminar viscosity, σ the diffusion constant, l_μ the length scale for turbulent momentum transfer and l_D the length scale for turbulent dissipation. In the absence of empirical information on turbulence for vortex flow, it is assumed that the turbulent diffusion constant and length scales can be deduced from the experimental data for two-dimensional flow on solid walls. This assumption is plausible, because the correct theory of vortex flow must be reducible to two-dimensional flow at large radius and zero circulation.

Experimental information on zero-pressure layers, examined by Hinze (1959), shows that the ratio of the turbulent shear velocity τ/ρ to the turbulent kinetic energy k is 0·3 on average, i.e.

$$\tau/\rho = 0{\cdot}3k. \tag{5}$$

The measurements of Klebanoff (1955) for the flow examined by Chi & Chang (1969) and Chi & Glowacki (1974) indicate that Prandtl's mixing length l, defined by the equation

$$\mu_t = \rho l(\tau/\rho)^{\frac{1}{2}}, \tag{6}$$

is given by

$$l = \begin{cases} L[0{\cdot}4(z/L) - 0{\cdot}5(z/L)^2 + 0{\cdot}2(z/L)^3][1 - \exp(-0{\cdot}05\rho(\tau/\rho)^{\frac{1}{2}} z/\mu)] & \text{for} \quad z < L, \\ 0{\cdot}1L \quad \text{for} \quad z \geqslant L, \end{cases} \tag{7}$$

where L is the boundary-layer thickness. Comparison of (2) and (6), bearing in mind the relationship (5) between τ/ρ and k, shows that $l_\mu = (0{\cdot}3)^{\frac{1}{2}}l$, hence with l given by (7), the form of l_μ for the present theory can be written as

$$l_\mu = \begin{cases} L[0{\cdot}219(z/L) - 0{\cdot}274(z/L)^2 + 0{\cdot}110(z/L)^3][1 - \exp(-0{\cdot}0274\rho k^{\frac{1}{2}}z/\mu) & \text{for } z < L, \\ 0{\cdot}055L \quad \text{for} \quad z \geqslant L. \end{cases} \tag{8}$$

For the dissipation length l_D, a further examination of the zero-pressure layer is made. It is now well-known, e.g. see Townsend (1961), that in such flows the balance between generation and dissipation of turbulent energy dominates, i.e. $\epsilon = \alpha$. For the zero-pressure layer the turbulent generation α is equal to $\rho\tau\,\partial u/\partial z$; α can therefore be derived in terms of ρ, k and l_μ from (2) and (5) as

$$\alpha = 0{\cdot}09\rho k^{\frac{3}{2}}/l_\mu, \tag{9}$$

and the turbulent dissipation is defined by (4). It then follows that $l_D = 11{\cdot}11l_\mu$ and hence from (8) we deduce that

$$l_D = \begin{cases} L[2{\cdot}434(z/L) - 3{\cdot}043(z/L)^2 + 1{\cdot}217(z/L)^3][1 - \exp(-0{\cdot}0274\rho k^{\frac{1}{2}}z/\mu)] & \text{for } z < L, \\ 0{\cdot}608L \quad \text{for} \quad z \geqslant L. \end{cases} \tag{10}$$

In order to determine the diffusion constant σ in (3), a two-dimensional linear-shear layer in the neighbourhood of solid wall, i.e. at small z, is examined. In such layer,

$$\tau/\rho = dP/dx. \tag{11}$$

Experimental data of Schubauer & Klebanoff (1951) under these conditions have been examined by Townsend (1961), who expressed the data in the form

$$u = 4(dP/dx)\,z^{\frac{1}{2}} + \text{constant}. \tag{12}$$

At small z our turbulent length scales (8) and (10) become

$$l_\mu = 0{\cdot}219z, \quad l_D = 2{\cdot}434z, \tag{13}$$

so the present turbulent energy equation (1) reduces under these conditions to

$$k^{\frac{3}{2}}/(2{\cdot}4342z) - d[(0{\cdot}219k^{\frac{1}{2}}/\sigma)\,dk/dz]/dz - (z\,dP/dz)^2/(0{\cdot}219zk^{\frac{1}{2}}) = 0. \tag{14}$$

The solution of this equation is easily shown to be

$$k = (z\,dP/dx)\,(0{\cdot}09 - 0{\cdot}072/\sigma)^{-\frac{1}{2}}. \tag{15}$$

Combination of this result with (10) and the shear stress for the flow under consideration,

$$\tau/\rho = 0{\cdot}219zk^{\frac{1}{2}}\,du/dz, \tag{16}$$

leads to an expression for the velocity u:

$$u = 9{\cdot}132(0{\cdot}09 - 0{\cdot}072/\sigma)^{\frac{1}{2}}\,(dP/dx)\,z^{\frac{1}{2}} + \text{constant}. \tag{17}$$

It can therefore be deduced by comparison of (12) and (17) that the diffusion constant σ is equal to 1·35.

From the foregoing consideration, we have established a turbulence model (1) for the vortex boundary-layer flow with μ_t, γ_t, ϵ, l_μ and l_D described by (2), (3), (4), (8) and (10)

respectively and σ equal to 1·35. The characteristic length L for the vortex boundary layer, which appears in (8) and (10), can be shown (e.g. see Chi, Ying & Chang 1969) to be equal to $r_0/(u^+r^+/\nu)^{\frac{1}{2}}$.

3. Governing equations and boundary conditions

Governing equations

On the basis of the turbulent model established above, the components of the stress tensor may be obtained by multiplying the corresponding components of the strain tensor by an effective viscosity μ_{eff} which is equal to the sum $\mu+\mu_t$ of the laminar and turbulent viscosities. Consequently the stress components for axisymmetric turbulent flow of an incompressible fluid assume the form

$$\left.\begin{aligned} \sigma_r &= -P+2\mu_{\text{eff}}\,\partial u/\partial r, & \tau_{r\theta} &= \mu_{\text{eff}}\, r\partial(v/r),\\ \sigma_\theta &= -P+2\mu_{\text{eff}}\,u/r, & \tau_{\theta z} &= \mu_{\text{eff}}\,\partial v/\partial z,\\ \sigma_z &= -P+2\mu_{\text{eff}}\,\partial w/\partial r, & \tau_{zr} &= \mu_{\text{eff}}(\partial u/\partial z+\partial w/\partial r), \end{aligned}\right\} \tag{18}$$

and the three momentum equations for the vortex flow are

$$\rho u\,\partial u/\partial r+\rho w\,\partial u/\partial z-\rho v^2/r = -\partial P/\partial r+r^{-1}\partial(2r\mu_{\text{eff}}\,\partial u/\partial r)/\partial r + \partial[\mu_{\text{eff}}(\partial u/\partial z+\partial w/\partial r)]\,\partial z-2\mu_{\text{eff}}\,u/r^2, \tag{19}$$

$$\rho u\,\partial v/\partial r+\rho w\,\partial v/\partial z+\rho uv/r = \partial(\mu_{\text{eff}}\,\partial v/\partial z)/\partial z+r^{-2}\partial[r^3\mu_{\text{eff}}\,\partial(v/r)/\partial r]/\partial r, \tag{20}$$

$$\rho u\,\partial w/\partial r+\rho w\,\partial w/\partial z = -\partial P/\partial z+\partial(2\mu_{\text{eff}}\,\partial w/\partial z)/\partial z+r^{-1}\partial[r\mu_{\text{eff}}(\partial u/\partial z+\partial w/\partial r)]/\partial r. \tag{21}$$

The continuity equation is

$$\partial ur/\partial r+\partial wr/\partial z = 0. \tag{22}$$

The stream function ψ, vorticity Ω and circulation Γ are defined as follows:

$$u = -r^{-1}\,\partial\psi/\partial z, \quad w = r^{-1}\,\partial\psi/\partial r, \tag{23}$$

$$\Omega = \partial u/\partial z-\partial w/\partial r, \quad \Gamma = rv. \tag{24), (25}$$

Equations of motion with the circulation, vorticity and stream function as the variable can be derived from (20), (19) and (21) and (22) respectively. It can be shown, e.g. see Gosman *et al.* (1969, p. 55) for two-dimensional flows in general and Chi & Jih (1974) for vortex flow in particular, that each of these equations as well as the turbulent energy equation has the form of the general elliptic equation

$$a\{\underbrace{\partial(\phi\,\partial\psi/\partial r)/\partial z-\partial(\phi\,\partial\psi/\partial z)}_{\text{Convection}}-\underbrace{\{\partial[br\,\partial(c\phi)/\partial z]/\partial z+\partial[br\partial(c\phi)/\partial r]/\partial r\}}_{\text{Diffusion}}+\underbrace{d}_{\text{Source}}=0, \tag{26}$$

where ϕ is the dependent variable, viz. Ω/r, Γ, ψ or k, and a, b, c and d stand for various functions, which are summarized in table 1.

In table 1, μ_t and μ_{eff} (defined as $\mu+\mu_t$) can be calculated from (2) and (8), and l_D from (10). Hence (26) represents four elliptical differential equations for four dependent variables: ψ, Ω/r, Γ and k, respectively. Integration of elliptical differential equations requires conditions on the variables on all field boundaries specified. These conditions are described below.

ψ	a	b	c	d
Ω/r	ρr^2	r^2	μ_{eff}	$-(\rho/r)\,\partial\Gamma^2/\partial z + 2r^2\{(\partial w/\partial z)\,\partial(\partial\mu_{eff}/\partial z)/\partial r - (\partial w/\partial r)\,\partial(\partial\mu_{eff}/\partial z)/\partial z + (\partial u/\partial z)\,\partial(\partial\mu_{eff}/\partial r)/\partial r - (\partial u/\partial z)\,\partial(\partial\mu_{eff}/\partial r)/\partial z\}$
Γ	ρ	$r^2\mu_{eff}$	$1/r^2$	0
ψ	0	$1/r^2$	1	$-r(\Omega/r)$
k	ρ/r	$r^{-1}(\mu+\mu_t/1{\cdot}35)$	1	$-4\mu_t\{\partial[r^{-1}(\partial\psi/\partial r)]/\partial z\}^2 - 4\mu_t\{\partial[r^{-1}(\partial\psi/\partial z)]/\partial r\}^2 - \mu_t\{\partial[r^{-1}(\partial\psi/\partial r)]/\partial r - \partial\{r^{-1}(\partial\psi/\partial z)\}^2 - \mu_t\{\partial[r^{-1}(\partial\psi/\partial z)]/\partial z\}^2 - \mu_t[r\,\partial(v/r)/\partial r]^2 + \rho k^{\frac{3}{2}}/l_D$

TABLE 1. The functions a, b, c and d.

Boundary conditions

The boundary conditions on the ground surface, the centre-line of the vortex and at a large radius from the centre-line can be derived from the requirements of physical continuity, axisymmetry of the flow and two-dimensionality of the vortex at a large radius, respectively. These conditions in terms of the vorticity, stream function, circulation and turbulent energy are as follows.

At $r = 0$,
$$\Omega/r = 8(\psi_1 r_2^2 - \psi_2 r_1^2)/r_1^2 r_2^2(r_2^2 - r_1^2), \tag{27a}$$
$$\psi = 0, \quad \Gamma = 0, \quad \partial k/\partial r = 0. \tag{27b–d}$$

At $r = r^+$,
$$\Omega/r = -r^{-2}(\partial^2\psi/\partial z^2 + \partial^2\psi/\partial r^2), \tag{28a}$$
$$\partial\psi/\partial r = 0, \quad \Gamma = \Gamma_{z=z^+}, \quad \partial k/\partial r = 0. \tag{28b–d}$$

At $z = 0$,
$$\Omega/r = -3\psi_1/(r^2 z_1^2) + \tfrac{1}{2}(\Omega/r)_1, \tag{29a}$$
$$\psi = 0, \quad \Gamma = 0, \quad k = 0. \tag{29b–d}$$

In the above equations, the subscripts 1 and 2 indicate values at grid points next and next by one, respectively, to the boundary under consideration; the superscript + indicates a value at the maximum height or radius, as appropriate, of the flow field under investigation. For brevity, details of the derivations of the above conditions are not presented here, but can be found in the paper by Chi & Jih (1974). However, care has been taken to specify upper boundary conditions at large z, say z^+, such that satisfactory matching of the present solution with the main vortex can be assured. Procedures for deriving the upper boundary conditions are described below.

It was shown by Deissler & Perlmutter (1960) for turbulent flow and by Lewellen (1962) for laminar flow that for a main vortex outside the boundary layer the most general form for ψ, in the present notation, is

$$\psi = F_0(r^2) + zF_1(r^2) \tag{30}$$

and Γ may be considered independent of z. Consequently, the following boundary conditions at large height have been derived from the definitions (23) and (24) of ψ and Ω respectively.

$$\text{At } z = z^+, \qquad \partial(\Omega/r)/\partial z = 4\partial^2 F_1/\partial(r^2)^2, \tag{31a}$$

$$\partial\psi/\partial z = F_1(r^2), \tag{31b}$$

$$\Gamma = \Gamma^+ \int_0^{r^2} \exp\left[-\int_0^{t^2} \frac{F_1}{2\nu_t r^2} dr^2\right] dt^2 \Big/ \int_0^{\infty} \exp\left[-\int_0^{t^2} \frac{F_1}{2\nu_t r^2} dr^2\right] dt^2, \tag{31c}$$

$$\partial k/\partial z = 0. \tag{31d}$$

It can be observed in the above equations that the gradients of ψ, Ω/r and k instead of the variables themselves have been chosen in the upper boundary conditions. The reason for this choice is that these values for the main vortex are dependent upon the boundary-layer flow, which is not known until after the boundary-layer solution has been obtained. On the other hand, the present gradient-type boundary conditions do not suffer from this defect.

4. Numerical procedure and computer program

For numerical integration of (26) with ψ, Ω/r, Γ and k as dependent variables, along with boundary conditions (27)–(29) and (31), the flow field in $0 \leqslant r \leqslant r^+$, $0 \leqslant z \leqslant z^+$ is represented by a rectangular grid system on a meridional (r, z) plane with

$$r_{i+1} = r_i + \Delta r_i \quad [i = 1\,(1)\,16], \tag{32}$$

$$z_{j+1} = z_j + \Delta z_j \quad [j = 1\,(1)\,16]. \tag{33}$$

The values of r^+ and z^+ are dependent upon the physical dimensions of the vortex and non-uniform grid spacings Δr_i and Δz_j have been used. Examples of these values can be found in §5. As will be seen in §5, the grid is finest in the region where the shear stresses vary most rapidly, i.e. near the ground surface and in the vortex core. All derivatives in the governing equations are replaced by algebraic differences involving the values of the dependent variables at the grid nodes. An upwind difference scheme for the elliptical equation (26) which was described in detail by the author and a co-worker (Chi & Jih 1974) in their studies of laminar vortex flow has been adapted by the author for this study.

The Gauss–Seidel successive iterative method, e.g. see Ames (1965), is used to solve the set of algebraic difference equations. This method is based upon using the improved values immediately in computing the improvements for the next grid node. However, the boundary conditions (27)–(29) and (31) are of two different types: the first specifies values of the variables themselves while the second specifies gradients. The former conditions are set at the beginning of the first iteration cycle and remain unchanged at successive iterations; the latter must be improved at the end of each iteration cycle.

A computer program in Fortran IV has been written to solve the algebraic difference equations using the iteration method described above. Before iteration starts, initial values are set: at the interior nodes all the variables are set to zero while the boundary values are calculated from (27)–(29) and (31). The first iteration cycle is then initiated. Each iteration cycle is subdivided into four subcycles in the order Ω/r, ψ, Γ and k. In each subcycle, calculation begins at the sixteenth column of the nodes (i.e. $i = 16$) with $j = 16(-1)\,2$, then the node values in the fifteen and fourteenth columns and so on are calculated until the second column has been calculated. Finally,

the boundary values are updated, using the gradient-type boundary conditions among (27)–(29) and (31). The above iteration cycle is then repeated until the preset convergence criterion (that all dependent variables for successive iterations agree to within 0·5 %) is met.

At the end of the iteration process, the values of Ω/r, ψ, Γ, k and μ_{eff} at the grid nodes are stored, and the velocity components u and w are recovered from the definition of ψ while v is recovered from that of Γ. The pressure $P_0 - P$, where P_0 is the value of P at $z = 0$, $r = r^+$, is then recovered through integration of the momentum equations (19)–(21).

When the program was first run considerable difficulty was experienced in attaining convergence of the turbulence energy k. This difficulty was overcome by developing a repeated under-relaxation procedure. In this procedure, instead of the newly calculated values of k, the previous k plus 0·2 of the difference between the current and the previous k is used as the new value of k in the calculation.

5. Discussion of results and comparison with experiments

Measurements of the horizontal components of the mean velocity distribution in the end-wall turbulent boundary layer of an intense vortex have recently been made by the author and a co-worker. Details of the experimental set-up (figure 2) were given by Chi & Costopolous (1974). Briefly, it consists of two annular cylinders of inner diameters 44·5 cm and 58·4 cm respectively, the thickness of the inner cylinder being 0·635 cm, and two end plates. The distance between the top and bottom plates is 91·4 cm. Compressed air was introduced into the annular space between the two cylinders and flowed into the inner cylinder through four columns of evenly pitched tangential holes (each column containing forty-eight 0·692 cm diameter holes 1·905 cm apart) drilled through the wall of the inner cylinder and subsequently discharged to the atmosphere through a 3·175 cm hole at the centre of the bottom plate. The horizontal component of the velocity and its direction in the vicinity of the top plate were measured by a directionally sensitive wedge-shaped hot-film probe. The hot film was on the axis of the cylindrical stem of the probe, and the probe was traversed axially through the top end plate at different radii so that the horizontal velocity at different r, θ and z could be measured. Figure 3 shows the measured radial distributions of u and v at large z (i.e. $z = 10$ cm) and figures 4(a) and (b) show the measured values of u and v, respectively, *vs.* z at several radii. Figure 3 also shows that the measured u and v distributions at large z, i.e. in the main vortex, can be correlated by the equations

$$u = -F_1(r^2)/r, \tag{34}$$

$$v = \Gamma_\infty \int_0^{r^2} \exp\left\{-\int_0^{t^2} [F_1(r^2)/2\nu_t r^2]\, dt^2\right\} dr^2 \Big/ \int_0^{\infty} \exp\{-F(r^2)/2\nu_t r^2]\, dt^2\}\, dr^2, \tag{35}$$

with
$$\Gamma_\infty = 27900, \quad F_1(r^2) = 2300[1 - \exp(-0{\cdot}000183 r^2)] \tag{36}$$

when cgs units are used.

As a numerical example, the present computer program has been used to calculate the end-wall boundary-layer flow under the same main vortex conditions as in the experiments. In this calculation, the function F_1 given in (36) has been employed to

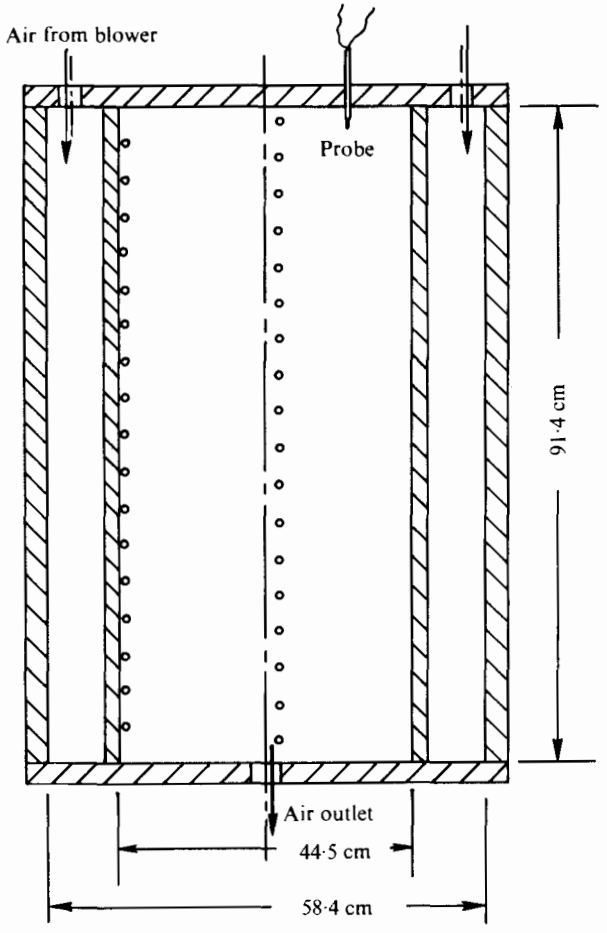

FIGURE 2. Schematic diagram of a laboratory vortex.

evaluate the boundary conditions (31) at $z = z^+$. The non-uniform grid system used in this calculation had

$$z = 0(0{\cdot}127)\,0{\cdot}762(0{\cdot}254)\,1{\cdot}27(0{\cdot}635)\,2{\cdot}54(1{\cdot}27)\,7{\cdot}62,\,10{\cdot}16\,\text{cm}, \tag{37}$$

$$r = 0(0{\cdot}635)\,3{\cdot}81(1{\cdot}27)\,7{\cdot}62(2{\cdot}54)\,20{\cdot}32,\,22{\cdot}25\,\text{cm}. \tag{38}$$

Figures 5, 6 and 7 show contour plots of the calculated stream function ψ, turbulent kinetic energy k and static pressure $P - P_0$. The calculated radial velocity u and tangential velocity v are plotted *vs.* z for several radii in figures 4 (*a*) and (*b*) for comparison with the experiments.

The ability of the present theory to correlate the measured mean velocity is demonstrated in figures 4 (*a*) and (*b*) by the excellent agreement between the theory and the experiments. In addition, several interesting boundary-layer characteristics may be observed in these figures. At large z and r, the tangential velocity dominates, as can be seen in figure 3; the force balance for this region is therefore characterized by a balance between the radial pressure gradient and the centrifugal force. Near the ground surface, retardation of the tangential velocity is seen in figure 4 (*b*). This retardation is

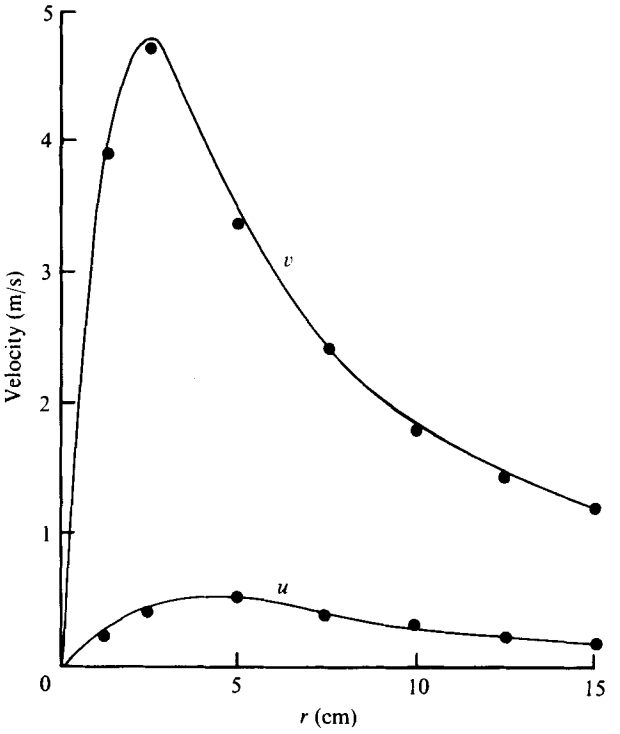

FIGURE 3. Tangential and radial velocities for the main vortex outside the boundary layer.

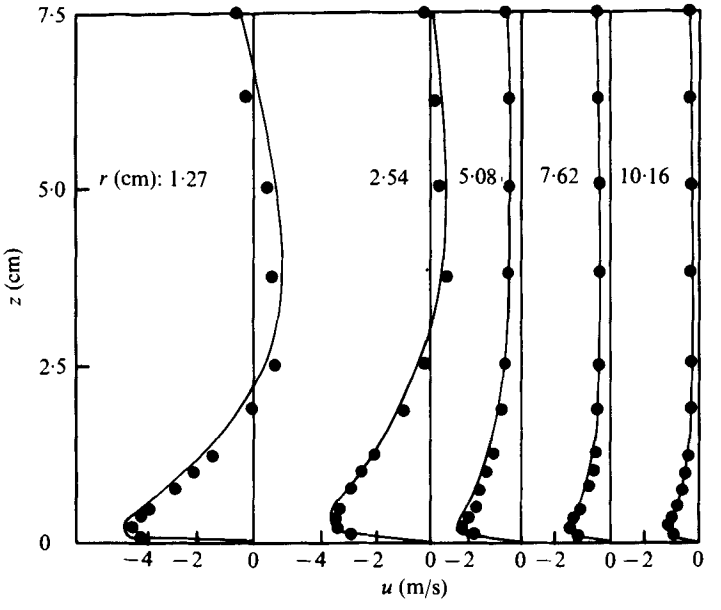

FIGURE 4(*a*). For legend see facing page.

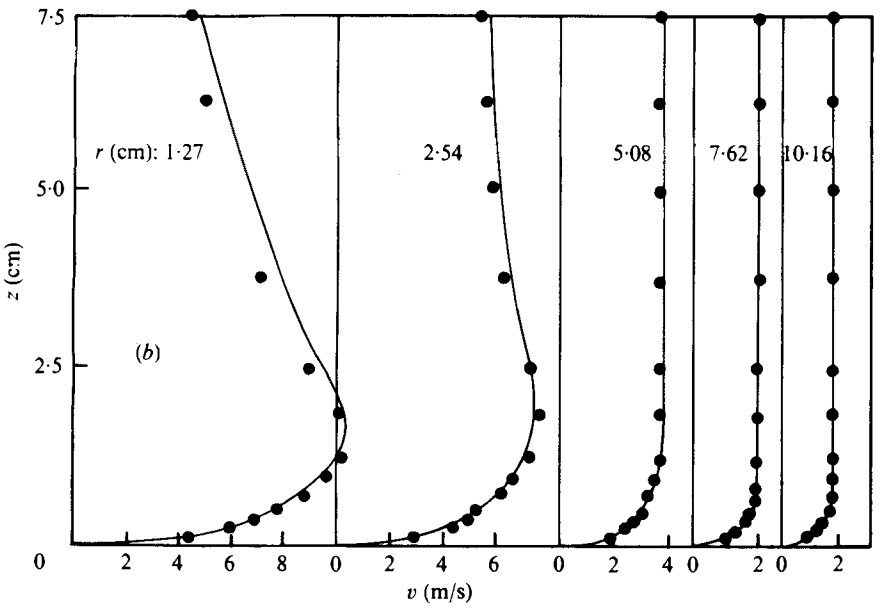

FIGURE 4. Measured and predicted values of (*a*) u and (*b*) v *vs.* z at several radii

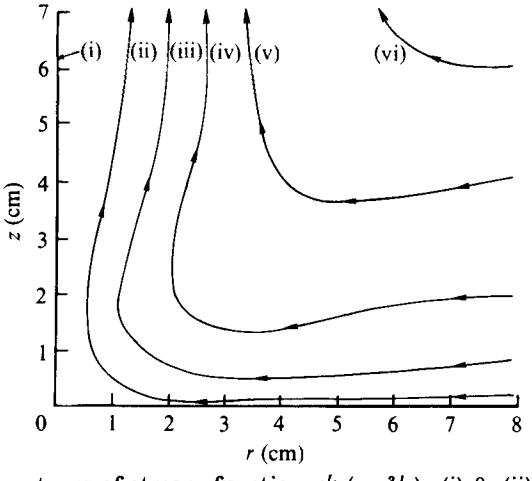

FIGURE 5. Predicted contours of stream function. ψ (cm^3/s): (i) 0, (ii) 150, (iii) 600, (iv) 1200, (v) 1700, (vi) 2000.

accompanied by a reduction in the centrifugal force; the balance between pressure and the centrifugal force is thereby destroyed. The flow in this region is thus characterized by the entrainment of fluid into the boundary layer as indicated by the deflexion of the streamlines towards the ground surface (see figure 5) and the large induced radial velocity u (see figure 4*a*). The eventual eruption of the entrained boundary-layer fluid at the vortex-core root can be seen in figure 5 from the streamlines at small r and z. In addition the entrained fluid carries circulation and turbulent energy from large radii to a position near the axis of symmetry, as can be seen in figure 4(*b*) from the large v and in figure 6 from the large k at small radius. For example, at $r = 1{\cdot}27$ cm the

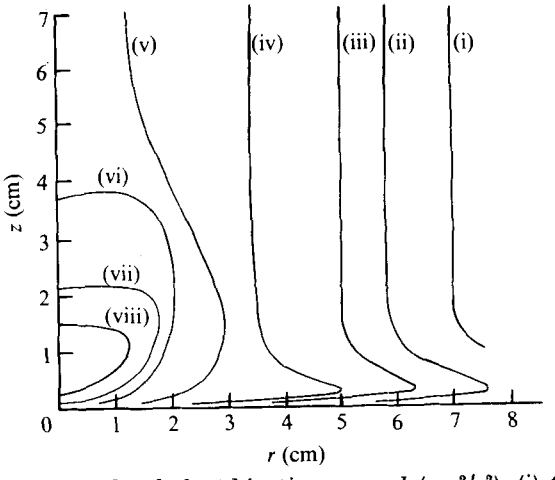

FIGURE 6. Predicted contours of turbulent kinetic energy. k (cm^2/s^2): (i) 400, (ii) 1000, (iii) 2000, (iv) 5000, (v) 10000, (vi) 20000, (vii) 50000, (viii) 75000.

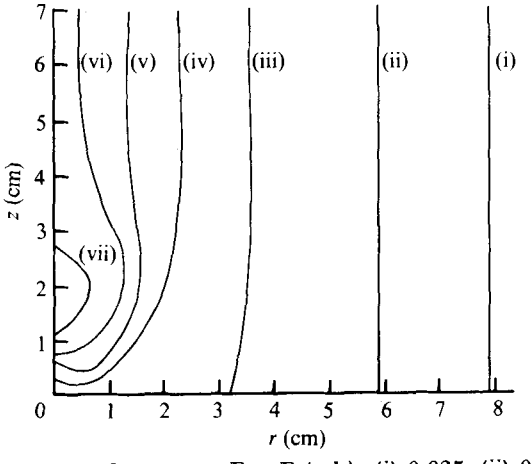

FIGURE 7. Predicted contours of pressure. $P_0 - P$ (mb): (i) 0·025, (ii) 0·05, (iii) 0·125, (iv) 0·25, (v) 0·35, (vi) 0·5, (vii) 0·7.

maximum tangential velocity in the boundary layer is 10·5 m/s, which is more than twice the maximum tangential velocity in the main vortex of 4·8 m/s. A high vacuum at the vortex core, for example at the centre of tornedo-like vortices, is well known. However, figure 7 indicates that the vacuum at the vortex-core root could be smaller than that at high altitude. This appears to be due to deceleration of the entrained fluid at the vortex-core root.

6. Summary and conclusions

A turbulence theory has been developed for the vortex end-wall boundary layer, which accounts for the generation at large radii of turbulent energy which diffuses and convects into the neighbourhood of the vortex-core root. This theory has been

incorporated into the equations of motion for the vortex boundary-layer flow. The resultant equations have been solved by a numerical method without simplifying assumptions. A procedure has also been developed for specifying boundary conditions for the main vortex such that satisfactory matching of the boundary-layer solution with the main flow can be assured.

The calculated horizontal components of the mean velocity are compared with values measured under the same conditions. The ability of the present theory to correlate the empirical data is shown to be good. In addition several interesting characteristics of the turbulent vortex boundary layer are predicted by the theory and discussed above. For example, (i) the vertical distribution of horizontal velocity is oscillatory in the inner region whilst it is of the ordinary boundary-layer type, without oscillation, in the outer region; (ii) the maximum velocity in the boundary layer can exceed the maximum velocity in the main vortex and (iii) the results contradict the general belief that the minimum pressure occurs in the vortex-core root.

This work was supported by the National Science Foundation under Grant GK 41469. The author wishes to express his appreciation to the Foundation. The author would also like to express his appreciation to Mr J. Jih and Mr T. Costopoulos for their assistance with computer programming and experimental measurements, respectively.

REFERENCES

AMES, W. F. 1965 *Nonlinear Partial Differential Equations in Engineering*, p. 377. Academic Press.

BÖDEWADT, W. T. 1940 Die Drehströmung über festem Grunde. *Z. angew. Math. Mech.* **20**, 241.

CHI, S. W. 1974 Numerical modelling of the three dimensional flows in the ground boundary layer of an intense axisymmetrical vortex. *Proc. S.E.S.* **10** (to be published).

CHI, S. W. & CHANG, C. C. 1969 Effective viscosity in a turbulent boundary layer. *A.I.A.A. J.* **10**, 2032.

CHI, S. W. & COSTOPOULOS, T. 1974 Measurements of mean velocity in turbulent vortex boundary layers. *Rep. to N.S.F.* GK 41469, 1974.

CHI, S. W. & GLOWACKI, W. J. 1974 Applicability of mixing length theory to turbulent boundary layers beneath intense vortices. *J. Appl. Mech.* **41**, 15.

CHI, S. W. & JIH, J. 1974 Numerical modeling of the three-dimensional flows in the ground boundary layer of a maintained axisymmetrical vortex. *Tellus* **26**, 444.

CHI, S. W., YING, S. J. & CHANG, C. C. 1969 The ground boundary layer of a stationary tornedo-like vortex. *Tellus* **21**, 693.

DEISSLER, R. G. & PERLMUTTER, M. 1960 Analysis of the flow and energy separation in a turbulent vortex. *J. Heat Mass Transfer* **1**, 173.

EMMONS, H. W. 1954 Shear flow turbulence. *Proc. U.S. Nat. Cong. Appl. Mech.* **2**, 1.

GLUSHKO, G. S. 1965 Turbulent boundary layer on a flat plate in an incompressible fluid. *Izv. Akad. Nauk SSSR, Mekh.* **4**, 13.

GOSMAN, A. D. *et al.* 1969 *Heat and Mass Transfer in Recirculating Flows.* Academic Press.

HINZE, J. O. 1959 *Turbulence*, p. 492. McGraw-Hill.

KLEBANOFF, P. S. 1955 Characteristics of turbulence in a boundary layer with zero pressure gradient. *N.A.C.A. Tech. Rep.* no. 1247.

KUO, H. L. 1971 Axisymmetric flows in the boundary layer of a maintained vortex. *J. Atmos. Sci.* **28**, 20.

LEWELLEN, W. S. 1962 A solution for three-dimensional vortex flow with strong circulation. *J. Fluid Mech.* **14**, 420.

MACK, L. M. 1964 The laminar boundary layer on a rotating disk of finite radius in a rotating flow. *JPL Space Prog. Summ.* no. 37–18, p. 43.

PRANDTL, L. 1945 Über ein neues Formelsystem für die ausgebildete Turbulenz. *Nachr. Akad. Wiss. Göttingen, Mathphys.* no. 6.

SCHUBAUER, G. B. & KLEBANOFF, P. S. 1951 Investigation of separation of the turbulent boundary layer. *N.A.C.A. Rep.* no. 1030.

SPALDING, D. B. 1967 Heat transfer from turbulent separated flows. *J. Fluid Mech.* **27**, 97.

STEWARTSON, K. 1957 On rotating laminar boundary layers. *Proc. Symp. Boundary Layer Res.* p. 59. Springer.

TOWNSEND, A. A. 1961 Equilibrium layer and wall turbulence. *J. Fluid Mech.* **11**, 97.